2008 IEEE International Conference on
Robotics and Automation
Pasadena, CA, USA, May 19-23, 2008

A System for Motion Control and Analysis of High-Speed Passively Twisting Flapping Wings

Daniel Watman and Tomonari Furukawa

Abstract— **This paper presents the design and evaluation of a system for motion control and analysis of high speed passively twisting flapping wings. The developed system is capable of flapping the wing under test with several controlled waveforms at frequencies up to 30 Hz, while capturing data about wing motion, lift force, and angle of attack. Performance was tested with sinusoidal, triangular, trapezoidal and square waveforms, with average position error below 5% for all cases up to and including 25 Hz. Wing control and data capture were found to be of high accuracy, and measurements showed significant differences in wing performance with different flapping motions, indicating a need for continuation of this research.**

I. INTRODUCTION

Micro aerial vehicles (MAVs) have recently become a research topic of great interest, with many potential applications in areas such as search and rescue, surveillance, and inspection of areas hazardous or inaccessible to humans. This has led to the investigation of alternative methods of propulsion such as flapping wings, which show potential for efficient, highly maneuverable MAVs at low Reynolds numbers. With recent advances in battery, motor, and electronic technologies it has become possible to build such vehicles, and the development of flapping wing MAVs has become a rapidly growing area of research.

Attempts to exactly imitate insects are not currently possible due to technological limitations, however analysis of insects provides valuable insight into some of the design characteristics of small-scale flapping wing flight [1]. Of particular interest is the wing motion of insects, and detailed analysis of this motion has been performed for several species [2], [3]. Dynamically scaled and computational models flapping in a similar motion to insects have allowed detailed measurement of flight forces and air flow, dramatically increasing our understanding of flapping wing flight [4], [5]. Use of these models also allows alternative flapping motions to be tested, and learning algorithms have been applied to determine optimal wing motion [6]. These studies concentrate on rigid wings and assume active control over wing trajectory and rotation, however this is extremely challenging to implement in a functional MAV, due to weight constraints and mechanical complexity.

The use of passively twisting wings, where the wing twists passively due to aeroelastic and inertial forces, is an alternative approach to lift generation. This method has the advantage of a simpler, lighter flapping mechanism, but lift may be reduced due to a suboptimal angle of attack throughout the stroke and imperfect timing of wing rotation, both of which have a significant effect on lift [7]. Flexible wings have also been demonstrated to have higher efficiency than rigid wings [8], and can be made more lightweight than a rigid wing of similar size. As a result of these advantages, the majority of successful flapping wing MAVs have made use of both flexible wings and passive twist, but have paid little attention to flapping motion, using a simple crank mechanism to generate roughly sinusoidal motion [9], [10], [11].

Previous studies have focused on flapping frequency and torsional stiffness [12], [13], but the effect of flapping motion on lift force and efficiency of passively twisting flapping wings has not been investigated in detail. Accurately scaling wing flexibility and inertia, as well as membrane properties, make it difficult to use a dynamically scaled model, and modeling these properties for computational analysis is also extremely challenging and computationally expensive. The previously mentioned studies use an experimental approach to overcome these problems, performing measurements on the actual wing being tested. A system capable of generating arbitrary flapping motions at high speeds is required to continue the investigation of passively twisting flapping wings.

This paper presents a new system for control and analysis of high-speed passively twisting flapping wings in air. The system is capable of flapping a wing with several different flapping motions over a range of frequencies, simultaneously recording data for analysis of the wing performance. In addition to wing trajectory, the lift force generated by the wing can be measured, and the aeroelastic deformation of the wing can be observed in real-time or photographed for later analysis. The combination of precise wing motion control and a range of measurements allows the currently unexplored effect of flapping motion on the performance of passively twisting flapping wings to be analyzed. This may lead to significant improvements in wing performance.

The following section presents the design of the developed control and analysis system. The procedure and parameters used to evaluate the system are then detailed. Finally, the measured performance of each part of the design is shown.

II. SYSTEM DESIGN

The developed motion control and analysis system consists of four main subsystems (Fig. 1): an embedded processor, a motion controller, lift measurement, and a visualization

This work was not supported by any organization

D. Watman and T. Furukawa are with the School of Mechanical and Manufacturing Engineering, The University of New South Wales, Sydney, 2052, Australia. d.watman@student.unsw.edu.au

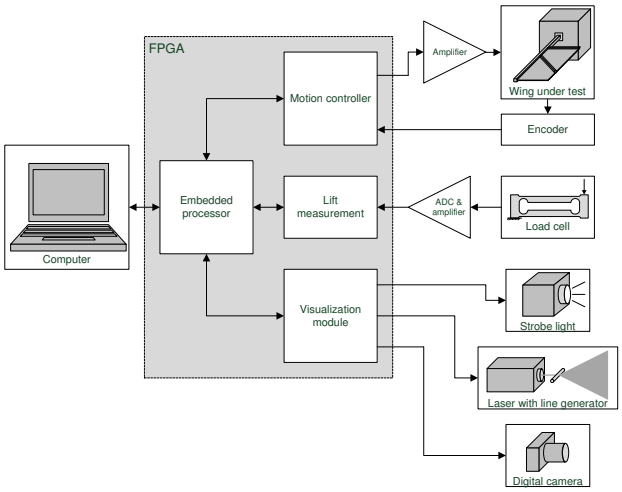

Fig. 1. System diagram

module. The system was implemented in a Xilinx Spartan-3E XC3S500E Field Programmable Gate Array (FPGA) for high speed parallel operation of the subsystems.

A. Embedded Processor

The embedded processor controls the overall operation of the system and manages the transfer of data to and from a PC, where operating modes and parameters are selected by the user. All adjustable parameters, including wing motion profiles, can be modified from the PC and updated at any time. Data such as lift measurement results can also be displayed in real-time or recorded for later analysis.

B. Motion Controller

As the desired trajectory of the wing is known in advance, the instantaneous position, velocity, and acceleration for each point in the flapping cycle are precalculated and stored in look-up tables in the FPGA. The look-up tables hold 1024 data points, which is sufficient for smooth motion without interpolation, and allows for complex flapping motions to be tested with a high degree of accuracy. The flapping frequency of the wing is changed by adjusting the rate at which the look-up table is incremented, and scaling the velocity and acceleration as required.

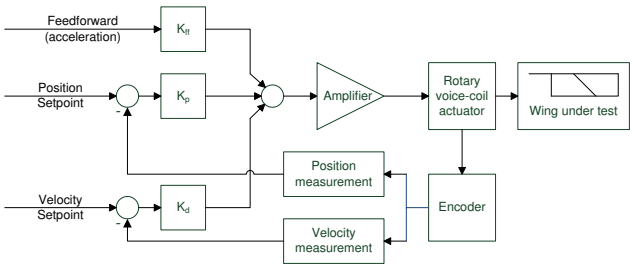

Fig. 2. PD controller with feedforward used to control the flapping wing

These parameters are then used as the inputs for a PD controller with feedforward as shown in Fig. 2. Due to parallel processing in the FPGA, the control output is calculated at an extremely high rate, however the position and velocity measurements are only updated each time the encoder, which is used for feedback, "ticks". The frequency of encoder ticks limits the effective sampling rate, which averages around 10 kHz for sinusoidal motion at 20 Hz. The output of the controller is a 10-bit PWM signal at 20 kHz, which is amplified and applied to the actuator through an L6205 full bridge driver.

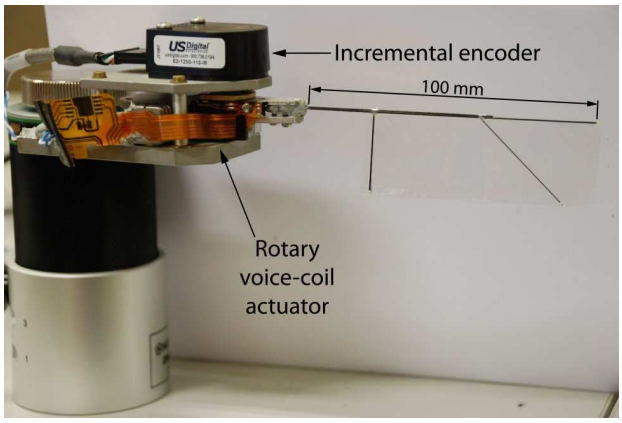

Fig. 3. Flapping mechanism and wing used for testing

The flapping mechanism shown in Fig. 3 consists of a rotary voice-coil actuator to drive the flapping wing, and a US Digital E2 1250 CPR incremental encoder for position and velocity feedback. The low friction and high acceleration of the voice coil actuator is necessary in order to flap the wing at high speeds with good controllability. A direct drive configuration was chosen to avoid the problem of backlash and allow fine control over the wing motion. The wing used for testing is made from 0.5 mm and 0.25 mm carbon pultrusions and 5 μm mylar film. The wing mounts directly onto the output arm of the actuator using a simple connection system that allows for easy connection and removal of wings.

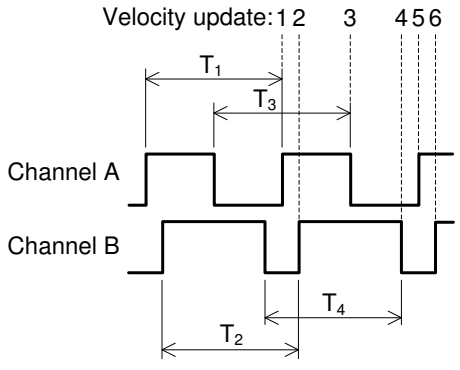

Fig. 4. Velocity measurement with uneven encoder channels

The velocity of the wing is calculated by measuring the period between encoder pulses, rather than measuring the

number of pulses in a fixed time period, to maximize accuracy and minimize latency. It was found that the width of the dark and light stripes on the encoder disk were not identical for both channels, so the period is measured between edges of the same type as shown in Fig. 4. These four periods are measured simultaneously and the most recent measurement is sent to the controller.

C. Lift Measurement

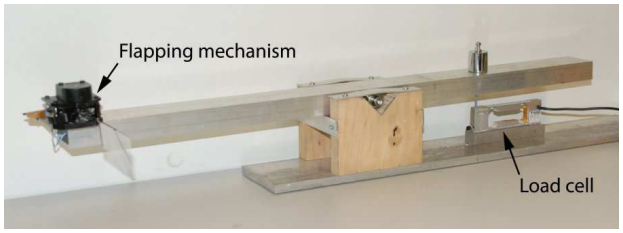

Fig. 5. Lift measurement hardware

A beam balance, instrumented with a Vishay model 1004 single point precision load cell, is used for measurement of average wing lift (Fig. 5). The flapping mechanism is mounted at 90° to the axis of the beam so that the lift force from the wing, which is distributed over the length of the wing, is at a consistent distance from the pivot point of the balance. This orientation, along with the relatively high mass of the beam, also helps to reduce vibrations which would otherwise affect the load cell and increase measurement noise. The force measurement was calibrated by placing standard weights on the pivot point of the wing, and zero readings were taken both before and after each lift measurement to correct for drift in the load cell.

The signal from the load cell is amplified using a Burr-Brown INA125 instrumentation amplifier, then low pass filtered and digitized with an Analog Devices AD7739 24-bit ADC at a sampling rate of 1 kHz. The digitized signal from the load cell is passed through a digital filter to recover the average lift measurement from the electrically and mechanically noisy signal. Currently a simple 1024 point average is used with satisfactory results, but there is the facility to use more complex filters if required.

D. Visualization Module

The visualization module is based on a previously developed system, which was designed to allow controlled real-time observation of a flapping wing in motion [14]. This module provides several operating modes for different visualization techniques:

1) Image capture: Still images of any phase position in the flapping cycle can be taken using a digital camera. Compensation for the camera shutter delay, with synchronized triggering of a strobe light or laser at the point of interest, allows highly accurate photographs to be taken.

2) Multi-triggering: The wing under test can be illuminated with a strobe light or laser at several points during the flapping cycle, for example to measure angle of attack at certain positions.

3) Real-time observation: For real-time observation of the wing, the source of illumination can be triggered each cycle at the same point for a continuous view of one wing position, or the trigger position can be smoothly varied for a slow motion view of the wing.

III. TEST SETUP

To evaluate the performance of the analysis system, a simple passively twisting wing was flapped at several frequencies between 15 and 30 Hz with several controlled waveforms. Each flapping motion was tested with a flapping amplitude of 15°, and measurements were taken of motion, lift force, power consumption, and wing angle of attack.

A. Tested Waveforms

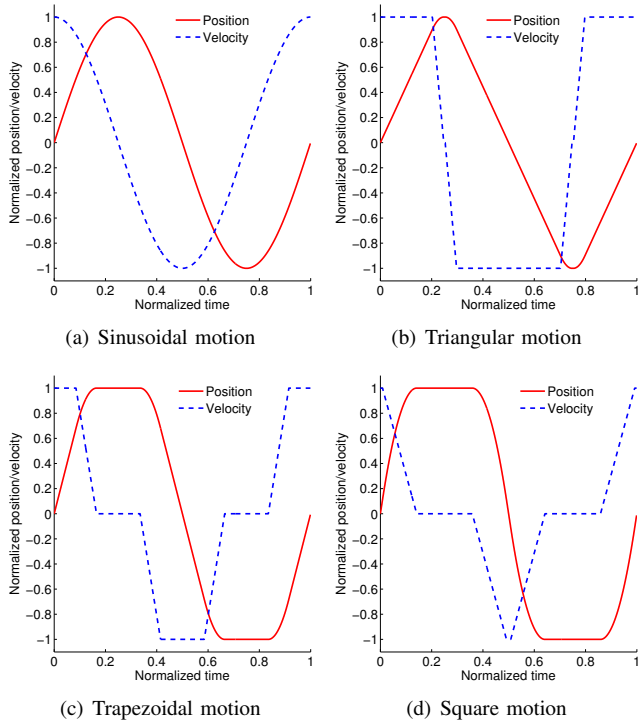

(a) Sinusoidal motion (b) Triangular motion

(c) Trapezoidal motion (d) Square motion

Fig. 6. Tested flapping motions

To evaluate the controller performance, four basic flapping motions were tested: sinusoidal, triangular, trapezoidal, and square. Instantaneous changes in velocity, such as the peaks in triangular motion, were smoothed with areas of constant acceleration, resulting in the waveforms shown in Fig. 6.

(a) Sinusoidal: Sinusoidal motion is the simplest and most commonly used oscillatory motion, so was tested as a basis for comparison with other waveforms.

(b) Triangular: The tested triangular motion consists of 90% constant velocity motion, with brief high acceleration changes of direction at the peaks. This motion is similar to the simplified insect wing motion mentioned previously.

(c) Trapezoidal: The trapezoidal motion used is a balance between the triangular and square waveforms. The velocity is zero for 50% of the motion, and in a constant velocity

transition period for the remaining 50% (neglecting the smoothed corners).

(d) Square: A true square wave is not possible to achieve in a flapping wing, so the tested waveform is similar to the trapezoidal motion, but with a sharper 30% transition time and no constant velocity section during the transition.

B. Data Acquisition

Measurements of wing trajectory and velocity were simultaneously recorded at a sampling rate of 2.5 kHz and buffered within the FPGA for downloading to a PC. Lift force measurements were sampled at 1 kHz and sent directly to a PC through an RS-232 connection for logging. Power measurement, not yet integrated into the analysis system, was calculated from averaged voltage and current measurements taken from the actuator driver circuit.

The wing cross section was illuminated 1 cm from the wingtip by a laser sheet, which was pulsed by the visualization module at 32 equally spaced phase positions throughout the flapping cycle. This allows the angle of attack of the wing to be observed, and was photographed and measured for each flapping motion.

IV. SYSTEM PERFORMANCE

A. Waveform Accuracy

TABLE I
MEASURED POSITION ERROR (%)
AVERAGE (ABOVE) AND MAXIMUM (IN BRACKETS)

Flapping motion	Frequency (Hz) 15	20	25	30
Sinusoidal	0.66 (3.77)	0.61 (1.65)	0.78 (2.03)	0.63 (1.86)
Triangular	0.43 (2.00)	0.95 (2.81)	0.84 (1.53)	2.36 (7.89)
Trapezoidal	0.89 (3.50)	1.08 (2.25)	1.42 (4.05)	4.23 (13.27)
Square	0.76 (2.50)	0.86 (3.60)	4.80 (17.64)	10.85 (30.07)

Table I shows the measured average and maximum position error for each waveform at the tested frequencies. The controller performance for the sinusoidal waveform is excellent, with an average error below 0.8% and a maximum error below 4% for all tested frequencies. The triangular and trapezoidal waveforms were also accurately produced up to 25 Hz, with average errors below 1.5% and maximum errors below 5%. At 30 Hz the maximum acceleration of the actuator began to cause significant error at the corners of the waveform, however the average error remained below 5%. The square waveform provided the most difficulty due to high accelerations, and there was visible lag in the high acceleration sections of the waveform at 25 Hz and above. The errors in the square waveform at 30 Hz were very high, reaching 30% in places, so the system is considered to be unable to perform this waveform.

B. Controller Performance

In addition to measurements of position error, detailed position and velocity data was recorded for each waveform. Data from each waveform at a flapping frequency of 25 Hz is shown below, as this is the highest frequency in which all waveforms were achievable. Measurements have been normalized to simplify comparison.

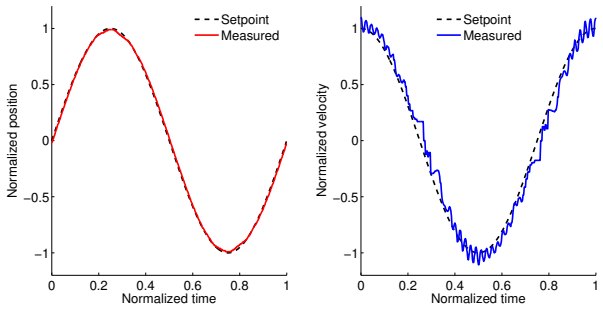

Fig. 7. Controller performance with sinusoidal motion at 25Hz

The sinusoidal waveform (Fig. 7) shows the recorded position and velocity at 25 Hz. The measured position closely matches the desired sinusoidal motion and the velocity, while containing high frequency oscillations, is also highly accurate. A small oscillation is visible at the peaks of the waveform where the velocity is close to zero. This is caused by the previously mentioned reduction in sampling rate at low velocities, which reduces the stability of the controller.

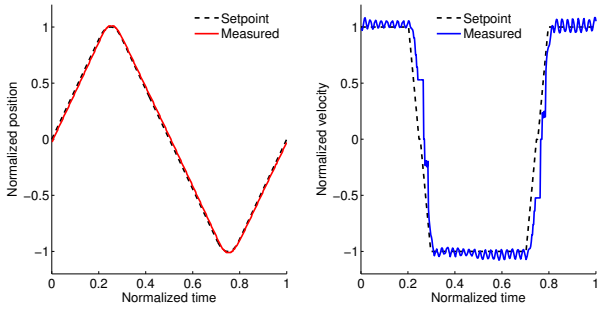

Fig. 8. Controller performance with triangular motion at 25Hz

The triangular waveform (Fig. 8) shares the high accuracy of the sinusoidal waveform. Although negligible on the position plot, a small oscillation at the areas of low velocity is present and can be seen in the velocity plot as areas of significant velocity error. The effect of this is minimal due to the small amount of time spent at low velocity.

The trapezoidal waveform (Fig. 9) contains areas of much higher velocity and acceleration than the previous waveforms, so a small amount of lag is visible in the constant velocity sections. A significant amount of time ideally spent at zero velocity causes noticeable oscillation, however the amplitude is only 2.5% of the full motion.

The square waveform (Fig. 9) has the highest velocity and acceleration of the tested waveforms, so has the highest error. A significant amount of lag is visible in the high

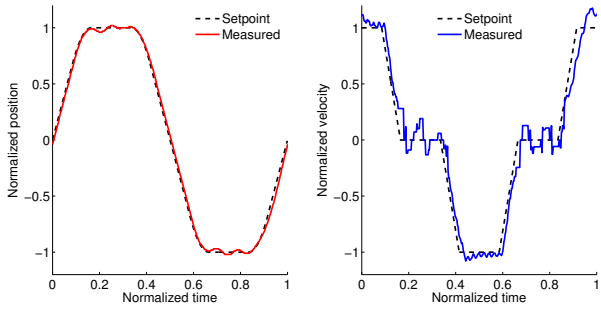

Fig. 9. Controller performance with trapezoidal motion at 25Hz

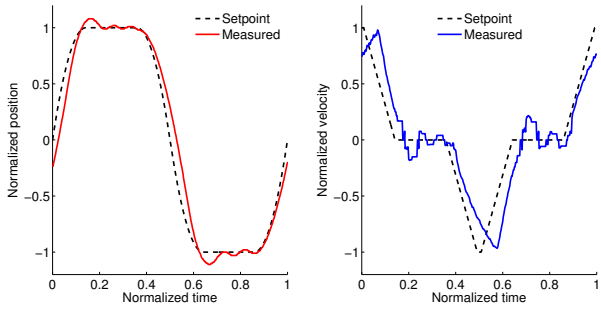

Fig. 10. Controller performance with square motion at 25Hz

velocity region, and the wing overshoots in addition to the oscillation in the flat part of the waveform. Also noticeable in the velocity plot is a decrease in acceleration as the velocity increases, probably due to back EMF from the voice-coil.

C. Lift Measurement

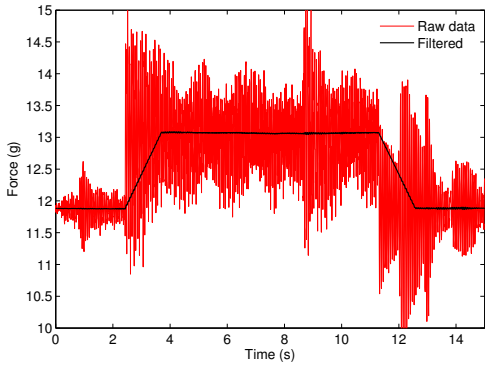

Fig. 11. Load cell data for trapezoidal motion at 30 Hz (wing active between t=3 and t=11 seconds)

Raw and filtered force measurements for trapezoidal motion at 30 Hz are shown in Fig. 11. The raw signal is extremely noisy, but the filtering process removes almost all noise. The remaining noise has an amplitude of approximately ± 0.01 g, which is an acceptable level compared to the lift force.

Fig. 12 shows lift and power measurements taken for all tested waveforms at several frequencies between 15 Hz and 30 Hz. The efficiency as a ratio of lift produced, divided by power required, is also shown. As the mechanism is designed

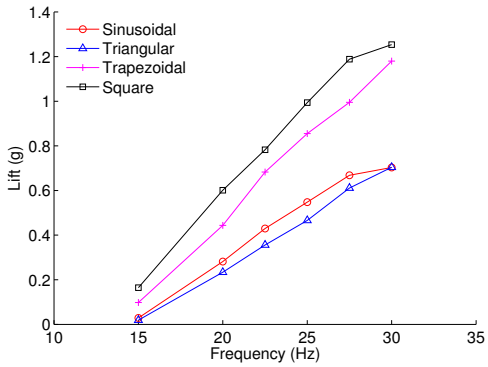

(a) Measured lift

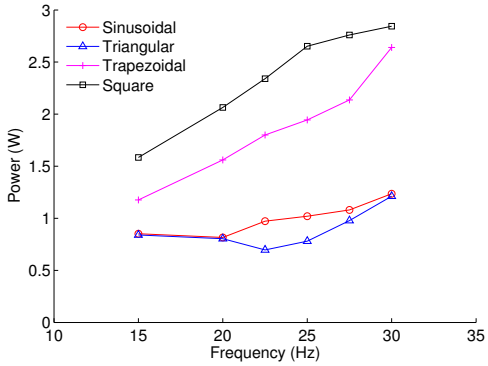

(b) Measured power

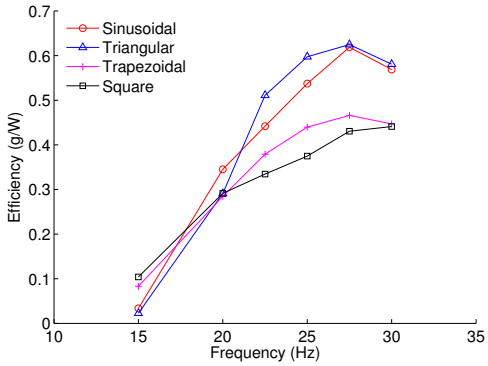

(c) Calculated efficiency

Fig. 12. Comparison of lift, power and efficiency between flapping motions

to test many different flapping motions this efficiency is quite low, but is useful for comparison between flapping motions. The lift increases linearly for all wing motions, with the exception of measurements at 30 Hz, however these measurements should be neglected as at this frequency the controller was unable to maintain all waveforms accurately. Surprisingly, the measurements all converge towards zero lift at slightly below 15 Hz, indicating that the wing stiffness could not be overcome at low frequencies and the resulting twist was negligible. The lift force generated by the square and trapezoidal waveforms was significantly higher than the sinusoidal and triangular waveforms, indicating a more favourable angle of attack. The sinusoidal and triangular waveforms performed similarly, with sinusoidal motion generating slightly more lift.

As expected, power consumption increased with frequency, and the waveforms with higher accelerations required more power. Interestingly, the sinusoidal and triangular waveforms had very similar power consumption at 15 Hz and 20 Hz, but above this the triangular waveform required less than the sinusoidal waveform. When the efficiency was calculated, this resulted in the triangular waveform being more efficient than the sinusoidal waveform over most of the frequency range tested. All waveforms appeared to peak in efficiency at around 27.5 Hz, suggesting wing resonance, but as the data at 30 Hz is unreliable, this peak may be slightly higher. At the efficiency peak, the sinusoidal and triangular waveforms were very close in efficiency, but overall the triangular waveform was found to be most efficient and the square waveform the most effective at producing lift.

D. Visualization

The visualization module was used to observe and record passive twisting of the wing for each waveform. Angle of attack at mid-stroke was measured manually from the resulting images.

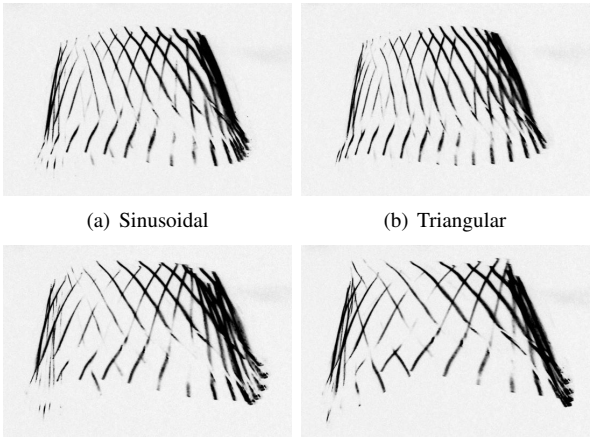

(a) Sinusoidal (b) Triangular

(c) Trapezoidal (d) Square

Fig. 13. Images of wing angle of attack taken by the visualization module at 25 Hz (leading edge at top)

TABLE II
MEASURED ANGLE OF ATTACK AT MID-STROKE (25 HZ)
TWIST ANGLE ALSO SHOWN FOR CLARITY

Angle (degrees)	Sinusoidal	Triangular	Trapezoidal	Square
Twist Angle	23	20.5	31.5	36.5
Angle of attack	67	69.5	58.5	53.5

Fig. 13 shows the images taken by the visualization module for each flapping motion at 25 Hz. The transparent wing membrane, illuminated by the laser sheet, is not visible in all positions due to irregular scattering, but differences can clearly be seen between the different flapping motions. The two waveforms with high speed transitions, trapezoidal and square, have significantly higher twist which corresponds to the higher lift measured for these waveforms. The twist angle measured at mid-stroke (Table II) is 36.5° for the square waveform, compared to 20.5° for the triangular waveform and results in more than double the lift force.

V. CONCLUSIONS AND FUTURE WORK

A new system for control and analysis of high-speed passively twisting flapping wings has been presented. Accurate control of the flapping motion was achieved for all tested waveforms up to 25 Hz, and measurements of lift force and angle of attack were successfully taken. Significant differences in lift and efficiency were found for the different flapping motions, indicating that wing motion is an important parameter for passively twisting flapping wings, and further investigation is warranted.

In a continuation of this research, a higher resolution encoder and an actuator capable of higher accelerations will be added, to increase both stability and the precision of control over the flapping motion. An integral term will also be added to the controller, further improving the accuracy of the waveform. This research is the first step towards an automated wing testing and analysis system for optimizing the design of passive flapping wings, and has the potential to increase the efficiency, flight time, and payload of flapping wing MAVs.

REFERENCES

[1] C.P. Ellington, The novel aerodynamics of insect flight: applications to micro-air vehicles, *Journal of Experimental Biology*, vol. 202(23), 1999, pp. 3439-3448.

[2] R. Dudley and C.P. Ellington, Mechanics of Forward Flight in Bumblebees: I. Kinematics and Morphology, *Journal of Experimental Biology*, vol. 148(1), 1990, pp. 19-52.

[3] S.N. Fry, R. Sayaman, and M.H. Dickinson, The Aerodynamics of Free-Flight Maneuvers in Drosophila, *Science*, vol. 300(5618), 2003, pp. 495-498.

[4] S.P. Sane, and M.H. Dickinson, The control of flight force by a flapping wing: lift and drag production, *Journal of Experimental Biology*, vol. 204(15), 2001, pp. 2607-2626.

[5] R. Ramamurti and W.C. Sandberg, A three-dimensional computational study of the aerodynamic mechanisms of insect flight, *Journal of Experimental Biology*, vol. 205(10), 2002, pp. 1507-1518.

[6] M. Motamed, J. Yan, "A Reinforcement Learning Approach to Lift Generation in Flapping MAVs: Experimental Results", *in IEEE International Conference on Robotics and Automation*, Roma, Italy, April 10-14, 2007, pp. 748-754.

[7] M.H. Dickinson, F.O. Lehmann, and S.P. Sane, Wing Rotation and the Aerodynamic Basis of Insect Flight, *Science*, vol. 284(5422), 1999, pp. 1954-1960.

[8] S. Heathcote, D. Martin, and I. Gursul, Flexible flapping airfoil propulsion at zero freestream velocity, *AIAA Journal*, vol. 42(11), 2004, pp. 2196-2204.

[9] T.N. Pornsin-Sirirak et al., "Microbat: A Palm-Sized Electrically Powered Ornithopter", *in Proceedings of NASA/JPL Workshop on Biomorphic Robotics*, Pasadena, CA, 2001.

[10] K.D. Jones, S.J. Duggan, M.F. Platzer, Flapping-wing propulsion for a micro air vehicle, *AIAA Paper 2000-0897*, 2000.

[11] D. Lentink, Novel Micro Aircraft Inspired by Insect Flight, *in International Symposium on Flying Insects and Robots*, Monte Verità, Switzerland, August 12-17, 2007, pp. 67-68.

[12] B. Singh et al., "Experimental Studies on Insect-Based Flapping Wings for Micro Hovering Air Vehicles", *in 46 th AIAA/ASME/ASCE/AHS/ASC Structures, Structural Dynamics, and Materials Conference*, 2005, pp. 1-19.

[13] C.S. Lin, C. Hwu, and W.B. Young, The thrust and lift of an ornithopter's membrane wings with simple flapping motion, *Aerospace Science and Technology*, vol. 10(2), 2006, pp. 111-119.

[14] D. Watman and T. Furukawa, "A System for Controlled Visualisation of Flapping Wings", *in International Symposium on Flying Insects and Robots*, Monte Verità, Switzerland, August 12-17, 2007, pp. 125-126.